Int. J. Solids Structures Vol. 26, No. 9/10, pp. 1099–1114, 1990
Printed in Great Britain.

0020–7683/90 $3.00+ .00

DECOHESION OF A CUT PRESTRESSED FILM ON A SUBSTRATE†

HENRIK M. JENSEN
Department of Solid Mechanics, The Technical University of Denmark, DK-2800 Lyngby, Denmark.

JOHN W. HUTCHINSON
Division of Applied Sciences, Harvard University, Cambridge, MA 02138, U.S.A.

and

KYUNG-SUK KIM
Division of Engineering, Brown University, Providence, RI 02912, U.S.A.

Abstract—Thin films or coatings on a substrate are often under a state of residual biaxial tension. This paper analyzes the cut test wherein a straight cut which is long compared to the film thickness is made through the film down to the substrate. Depending on the elastic properties of the materials, the residual stress level, and the toughness of the interface bond between the film and substrate, the cut may induce extensive decohesion, limited decohesion or no decohesion at all. The main thrust of this paper is concerned with the shape and extent of the zone of decohesion when extensive decohesion occurs. The interface crack front at the boundary of the decohered region is subject to mixed mode conditions involving modes 1, 2 and 3. The shape of the decohesion region depends sensitively on the way in which the mode 3 contribution enters the decohesion criterion. Observations of shapes for a polyimide film on a glass substrate permit the relative importance of the mode 3 contribution to be inferred when the decohered film makes no contact with the substrate. Some experimental observations indicate that the decohesion process is quite complex when the decohered film makes contact with the substrate. A prototypical criterion for mixed mode interfacial fracture is proposed for cases in which the interfacial crack remains open.

1. INTRODUCTION

A thin film or coating bonded to a substrate and under a state of residual biaxial tension will decohere starting from a flaw at a free edge or from a through-cut if the residual stress is sufficiently high and/or the bond is sufficiently weak (Evans *et al.*, 1988). If the substrate has low toughness compared to the interface, cracking may occur in the substrate (Evans *et al.*, 1988; Suo and Hutchinson, 1989b), but that possibility is not considered here. Suppose the film is in a state of equal biaxial tension σ and suppose the film thickness t is very small compared to the substrate thickness so that the substrate can be considered to be infinitely thick. Let E, μ and ν be Young's modulus, shear modulus and Poisson's ratio of the film and E_s, μ_s and ν_s be the corresponding quantities for the substrate. The energy release rate, $\mathcal{G}$, of a two-dimensional plane strain crack on the interface and emerging from a through-cut is shown in Fig. 1. This result was obtained by Thouless *et al.* (1989) using finite element techniques for the case where the elastic properties of the substrate coincide with those of the film. When the interface crack is longer than 3 to 5 film thicknesses it approaches steady-state conditions with a length-independent energy release rate given by

$$\mathcal{G} = \frac{1}{2}\frac{1-\nu^2}{E}\sigma^2 t. \tag{1}$$

This steady-state result is independent of the elastic properties of the substrate.

The plane strain interface crack is characterized by two stress intensity factors, K_1 and K_2, such that on the interface a distance r ahead of the tip the normal and shear stresses are given by

†Dedicated to the memory of Charles D. Babcock.

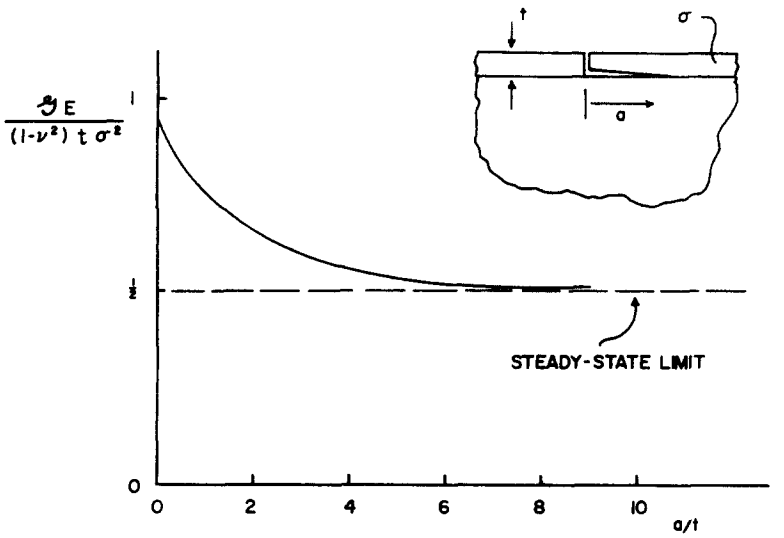

Fig. 1. Sketch of the variation of energy release rate $\mathcal{G}$ for a plane strain interface crack spreading from a cut in a film with residual biaxial tension σ. See Thouless *et al.* (1989) for an accurate plot.

$$(\sigma_{22}, \sigma_{12}) = (K_1, K_2)\,(2\pi r)^{-1/2}. \tag{2}$$

The two Dundurs parameters measuring the elastic mismatch between the film and the substrate are

$$\alpha = \frac{E/(1-\nu^2) - E_s/(1-\nu_s^2)}{E/(1-\nu^2) + E_s/(1-\nu_s^2)}, \quad \beta = \frac{1}{2}\,\frac{\mu(1-2\nu_s) - \mu_s(1-2\nu)}{\mu(1-\nu_s) + \mu_s(1-\nu)}. \tag{3}$$

In writing (2) it has been assumed that $\beta = 0$ (either exactly or as an approximation), and thus we are sidestepping some of the difficulties associated with the more pathological oscillatory interface singularity. Throughout the paper we will take $\beta = 0$. Under this circumstance and under combined mode 1 and 2,

$$\mathcal{G} = \frac{1}{2}\left(\frac{1-\nu^2}{E} + \frac{1-\nu_s^2}{E_s}\right)(K_1^2 + K_2^2) \tag{4}$$

assuming $K_1 > 0$ so that the crack is open. The steady-state plane strain problem for decohesion driven by a tensile stress σ has $K_1 > 0$ but is heavily mixed mode with the phase of the stress intensity factors, $\psi = \tan^{-1}(K_2/K_1)$, depending on α as shown in Fig. 2 (Hutchinson, 1989; Suo and Hutchinson, 1989a).

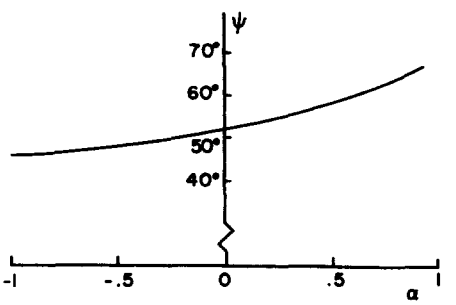

Fig. 2. Dependence of the phase of the stress intensity factors, $\psi = \tan^{-1}(K_2/K_1)$ for a steady-state plane strain interface crack as a function of the elastic mismatch parameter α when $\beta = 0$. The crack is driven by residual tensile stress in the thin film.

In general, interface toughness is strongly mode-dependent (Cao and Evans, 1988), usually with the energy release rate needed to drive the crack increasing with increasing proportion of mode 2 to mode 1. The condition for decohesion of a plane strain crack can be written as

$$\mathcal{G} = \mathcal{G}_c(\psi) \tag{5}$$

where $\mathcal{G}_c(\psi)$ is the mode-dependent interface toughness which must be determined by test. The critical stress associated with steady-state plane decohesion from (1) and (5) is

$$\sigma_c = \left(\frac{2E\mathcal{G}_c(\psi)}{(1-\nu^2)t}\right)^{1/2} \tag{6}$$

where ψ is found from Fig. 2.

The general criterion (5) includes two limiting cases which will be considered later. An "ideally brittle" interface is defined as an interface with a mode-independent toughness, i.e.

$$\mathcal{G}_c(\psi) = \mathcal{G}_c^0. \tag{7}$$

One imagines that the total energy released goes into the creation of the new surfaces. At the other extreme, consider an interface crack where the tip is fully shielded from any effect of K_2; that is, assume the condition for crack advance is $K_1 = K_1^c$, independent of K_2. The fully shear-shielded criterion is

$$\mathcal{G}_c(\psi) = \mathcal{G}_c^0/\cos^2\psi \tag{8}$$

where $\mathcal{G}_c^0$ is the pure mode 1 toughness related to K_1^c by (4). Experimental data for an epoxy/glass interface obtained by Cao and Evans (1989) over a wide range of modes 1 and 2 fell somewhat below the trend of (8) and well above (7). Using micromechanical modeling, Evans and Hutchinson (1989) produced a family of criteria for combined mode 1 and 2 interface fracture which depended on a single nondimensional parameter characterizing the roughness of the failed interface. Their family of criteria reduced to (7) for a perfectly smooth interface and to (8) in the limit of a very rough interface.

In the cut test, a straight cut of length $2L$, which is very long compared to the film thickness, is made through the film to the substrate. If consideration is limited to purely elastic behavior in the film and substrate and if substrate cracking does not occur, there are three response regimes as depicted in Fig. 3. Let σ_i be the lowest value of σ needed to initiate decohesion at the intersection of the through-cut and the interface. Usually, σ_i will be less than σ_c (c.f. Fig. 1), although, in general, the size of σ_i relative to σ_c will depend on α and on the ψ-dependence of $\mathcal{G}_c(\psi)$. If $\sigma_i < \sigma_c$, as assumed in Fig. 3, then no decohesion can occur if

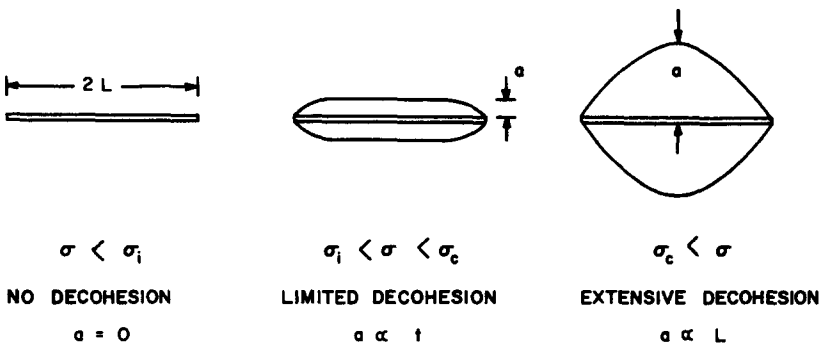

Fig. 3. Three regimes of behavior for cut test when $\sigma_i < \sigma_c$.

$$\sigma < \sigma_i. \tag{9}$$

If

$$\sigma_i < \sigma < \sigma_c \tag{10}$$

the extent of the decohered region from the cut in its central portion will be determined by a plane strain relation such as that in Fig. 1 and will be limited to distances perpendicular to the cut on the order of, typically, 1 to 5 times t. If

$$\sigma > \sigma_c \tag{11}$$

there will be extensive decohesion spreading out over an area controlled by the length of the cut. For material combinations for which $\sigma_i > \sigma_c$, there are two response regimes: $\sigma < \sigma_i$ with no decohesion and $\sigma > \sigma_i$ with extensive decohesion.

2. MODEL OF THE CUT TEST ($\sigma > \sigma_c$)

The regime of extensive decohesion is considered with $\sigma > \sigma_c$ (and $\sigma > \sigma_i$ if $\sigma_i > \sigma_c$). If $L \gg t$, it can be anticipated that the extent of the decohesion perpendicular to the cut will be determined by L and will be very large compared to t. For one experimental system discussed in Section 4, the lateral extent of the decohered region is about one hundred times t. The stress distribution in the cut decohered film is analyzed as a two-dimensional plane stress problem. Assume for the moment that the boundary C of the decohered region is known. As depicted in Fig. 4, the stress distribution within the decohered region of the cut film is the sum of the stresses in two plane stress problems, (i) and (ii). Problem (i) is the trivial uniform equal biaxial stress state σ and Problem (ii) is the plane stress distribution for a film clamped along C and subject to a normal traction σ along the cut, i.e.

$$\begin{aligned} &u_1 = u_2 = 0 && \text{on } C \\ &\sigma_{12} = 0 \quad \text{and} \quad \sigma_{22} = -\sigma && \text{on } x_2 = 0, |x_1| < L. \end{aligned} \tag{12}$$

The boundary C of the decohered region has been depicted as standing off the ends of the cut in Fig. 4. Whether the boundary stands off or is attached to the ends of the cut turns out to be a significant issue which is tied to the details of the interface decohesion criterion. This issue will be dealt with in Section 3.

The stresses in the film resolve into a normal component, σ_{nn}, and a tangential component, σ_{nt}, to the boundary C as shown in Fig. 5. The steady-state energy release rate for a *straight* crack front when the film has *uniform* normal and tangential stresses is, instead of (1),

$$\mathcal{G} = \frac{1}{2}\frac{(1-\nu^2)}{E}\Delta\sigma_{nn}^2 t + \frac{1}{2}\frac{1}{\mu}\Delta\sigma_{nt}^2 t \tag{13}$$

where $\Delta\sigma_{nn}$ and $\Delta\sigma_{nt}$ are the stress *changes* from the state of biaxial tension σ. Equation

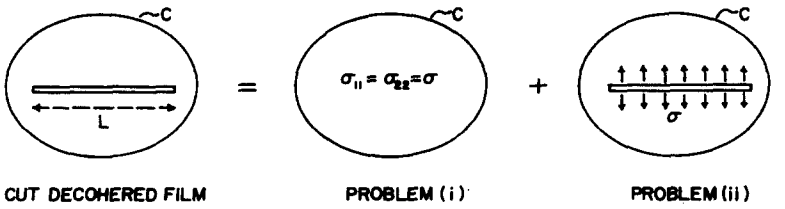

Fig. 4. Plane stress model of extensive decohesion when $\sigma > \sigma_c$. Problem (i) is state of uniform biaxial tension σ. Problem (ii) has clamped boundary C with normal traction σ applied to cut.

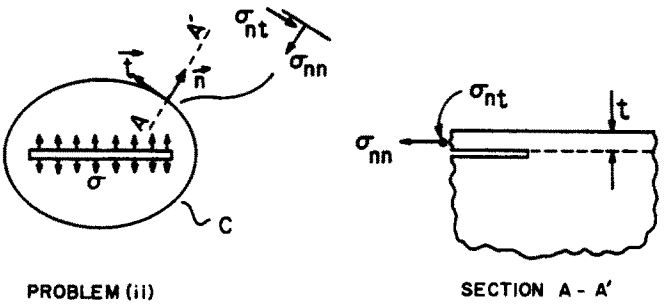

Fig. 5. Local tractions σ_{nn} and σ_{nt} in film along interface crack front for Problem (ii).

(13) holds locally along the crack front if the radius of curvature of C and the length scale over which $\Delta\sigma_{nn}$ and $\Delta\sigma_{nt}$ vary are large compared to the film thickness t. This is assumed to be the case in the present model, and the stress changes $\Delta\sigma_{nn}$ and $\Delta\sigma_{nt}$ are calculated from the stresses in Problem (ii).

Locally along the crack front C, $\Delta\sigma_{nn}$ induces mode 1 and mode 2 with K_2 and K_1 in *fixed* proportion characterized by ψ in Fig. 2, while $\Delta\sigma_{nt}$ induces mode 3. Under the three modes of loading the energy release rate is related to the stress intensity factors by (with $\beta = 0$)

$$\mathcal{G} = \frac{1}{2}\left(\frac{1-\nu^2}{E} + \frac{1-\nu_s^2}{E_s}\right)(K_1^2+K_2^2) + \frac{1}{4}\left(\frac{1}{\mu}+\frac{1}{\mu_s}\right)K_3^2. \tag{14}$$

Thus, by comparing (13) and (14), one has

$$\left(\frac{1-\nu^2}{E} + \frac{1-\nu_s^2}{E_s}\right)(K_1^2+K_2^2) = \left(\frac{1-\nu^2}{E}\right)\Delta\sigma_{nn}^2 t \tag{15}$$

and

$$\frac{1}{2}\left(\frac{1}{\mu}+\frac{1}{\mu_s}\right)K_3^2 = \frac{1}{\mu}\Delta\sigma_{nt}^2 t \tag{16}$$

where $\psi = \tan^{-1}(K_2/K_1)$ is given by Fig. 2. The above assumes $K_1 > 0$, which holds if $\Delta\sigma_{nn} < 0$. If $\Delta\sigma_{nn} \geqslant 0$, the crack front does not open, $K_1 = 0$, and (14) and (15) apply with $K_1 = 0$ if the fractured interface is perfectly smooth with no friction.

We now propose a family of criteria governing the advance of the interface crack between the film and the substrate. Since the relative proportion of K_2 to K_1 is fixed along the front, the shape of the decohered region is not dependent on how ψ enters into the decohesion criterion. Put another way, the observed shape of a decohered region cannot be used to discriminate how the relative proportions of K_2 to K_1 enter the decohesion criterion. As will be seen, however, the shape is strongly dependent on the way in which the mode 3 intensity factor is included in the criterion.

Noting (13), consider the family of criteria specified by

$$\frac{1}{2}\frac{(1-\nu^2)}{E}\Delta\sigma_{nn}^2 t + \lambda\frac{1}{2}\frac{1}{\mu}\Delta\sigma_{nt}^2 t = \mathcal{G}_c^* \tag{17}$$

where $\mathcal{G}_c^*$ can be thought of as the critical energy release rate for the plane strain crack in (5) when $\Delta\sigma_{nt} = 0$, i.e. $\mathcal{G}_c^* = \mathcal{G}_c(\psi)$. The parameter λ in (17) is used to adjust the influence of the mode 3 contribution. When $\lambda = 0$, mode 3 has no effect on the condition for crack advance—the crack tip is fully shielded from any influence of mode 3. At the other limit,

$\lambda = 1$, there is no shielding of the crack tip from mode 3. This family of criteria includes the "ideally brittle" interface if $\lambda = 1$ and $\mathcal{G}_c^*$ is identified with $\mathcal{G}_c^0$ in (7). The limit of an interface fully shielded from both mode 2 and mode 3 is also included in (17) if $\lambda = 0$ and $\mathcal{G}_c^*$ is identified with $\mathcal{G}_c(\psi)$ in (8).

When the decohered region remains attached to the ends of the cut, the computed distribution of $\Delta\sigma_{nn}$ along C reported in Section 4 is everywhere negative giving $K_1 > 0$ along the front. When, on the other hand, the decohered region stands off the ends of the cut it is found that there is a small portion of C just opposite the ends where $\Delta\sigma_{nn}$ turns out to be positive implying that the crack is closed along this portion of its front. The steady-state energy release rate (13) still applies when $\Delta\sigma_{nn} > 0$, assuming friction effects are not important, and a criterion in the form of (17) remains plausible. However, one should not necessarily expect the same values of the parameters λ and $\mathcal{G}_c^*$ to hold for both $\Delta\sigma_{nn} < 0$ and $\Delta\sigma_{nn} > 0$. Nevertheless, in the present exploratory study we have used (17) independent of the sign of $\Delta\sigma_{nn}$. The limitations of this assumption for the case in which the decohered region stands off the end of the cut will be discussed in Section 5 along with some experimental evidence which suggests that an adequate criterion is probably lacking when contact between the decohered film and the substrate takes place.

In Appendix A, we propose a class of criteria for characterizing interfacial fracture under combined three-mode conditions, of which (17) is a special case. In Appendix A, the general class of criteria, including the special family (17), are expressed as

$$\mathcal{G} = \mathcal{G}_c(\psi, \phi) \tag{18}$$

where ψ and ϕ are Euler angles in a space of (K_1, K_2, K_3). In the present study, (17) is the convenient form for the decohesion criterion.

We now summarize the model for predicting the shape of the decohered region when $\sigma > \sigma_c$, where in the new notation used in (17)

$$\sigma_c = \left(\frac{2E\mathcal{G}_c^*}{(1-\nu^2)t}\right)^{1/2}. \tag{19}$$

The plane stress boundary value problem for determining the boundary C of the decohered region is Problem (ii) of Fig. 4 with boundary conditions (12). The boundary C must be found such that (17) is satisfied everywhere along C, where $\Delta\sigma_{nn}$ and $\Delta\sigma_{nt}$ are the normal and tangential tractions to C determined from Problem (ii). This assumes that the interface crack is poised for continuing advance at every point along C and has nowhere become subcritical. This is a reasonable assumption for a decohering region spreading from a lengthening cut and is consistent with the shapes produced in Section 4. Alternatively, one could cut the film when $\sigma < \sigma_c$ and then increase σ above σ_c, for example by changing temperature and exploiting thermal expansion mismatch between the film and substrate. In this case, too, one can reasonably expect that the crack front will advance simultaneously everywhere along C as the temperature is changed. By (19), condition (17) can be rewritten as

$$\sigma_{nn}^2 + \frac{2\lambda}{(1-\nu)}\sigma_{nt}^2 = \sigma_c^2 \tag{20}$$

where σ_{nn} and σ_{nt} are the stresses in Problem (ii).

From dimensional considerations and the form of (20), it is readily concluded that the *shape* of the decohered region depends only on

$$\sigma/\sigma_c, \lambda \text{ and } \nu \tag{21}$$

while the *size* scales with the length of the cut, $2L$.

3. LOCAL ANALYSIS AT THE END OF THE CUT

Observations of the cut test indicate that in some instances the decohesion boundary C remains attached to the end of the cut while for some other material combinations it stands off the end of the cut. Insight into this issue is gained by investigating the conditions under which the boundary can be attached. Consider the local geometry shown in Fig. 6 where the boundary emerges from the end of the cut at an angle ω. Let (r, θ) be planar-polar coordinates centered at the cut end, and look for a solution to the plane stress boundary value problem for the wedge region of Fig. 6 where the stresses depend on θ but not on r. Such a solution is readily found. Along the rigidly clamped edge on $\theta = \omega$ the stresses are found to be

$$\begin{aligned}
\sigma_{\theta\theta} &= -2\sigma\cos 2\omega[1-\nu+(1+\nu)\cos 2\omega]^{-1} \\
\sigma_{r\theta} &= -\sigma(1-\nu)\sin 2\omega[1-\nu+(1+\nu)\cos 2\omega]^{-1} \\
\sigma_{rr} &= \sigma[1-\nu-(1+\nu)\cos 2\omega][1-\nu+(1+\nu)\cos 2\omega]^{-1}.
\end{aligned} \tag{22}$$

A separate calculation for the wedge region of Fig. 6 with homogeneous boundary conditions (i.e. with $\sigma_{\theta\theta} = -\sigma$ replaced by $\sigma_{\theta\theta} = 0$ on $\theta = 0$), shows that the stresses from the homogeneous problem will approach zero as $r \to 0$ as long as

$$1-\nu+(1+\nu)\cos 2\omega > 0. \tag{23}$$

That is, the most singular admissible stresses to the homogeneous problem vanish as $r \to 0$ when (23) is met. (For $\nu = 1/3$, (23) requires $\omega < 60°$, while for $\nu = 1/2$, $\omega < 54.7°$.) Thus for a boundary emerging from the cut with an angle ω satisfying (23), the local stresses along the boundary on $\theta = \omega$ are given by (22).

Now consider the requirement that (20) be satisfied along $\theta = \omega$. With $\sigma_{nn} = \sigma_{\theta\theta}$ and $\sigma_{nt} = \sigma_{r\theta}$ from (22), (20) becomes

$$F(\omega, \lambda) = (\sigma_c/\sigma)^2 \tag{24}$$

where

$$F(\omega, \lambda) = [4\cos^2 2\omega + \lambda(1-\nu)\sin^2 2\omega]/[1-\nu+(1+\nu)\cos 2\omega]^2. \tag{25}$$

A plot of F as a function of ω for various λ is shown in Fig. 7 for $\nu = 1/3$.

Next, recall that the regime of extensive decohesion under consideration requires $\sigma > \sigma_c$ so that the right hand side of (24) is less than unity. The angle ω made by the boundary satisfying (24) is given by the intersection of the solid-line curve in Fig. 7 (for a given λ) with the dashed-line curve for a given σ/σ_c, as illustrated in Fig. 7. The solution where the dashed-line intersects the solid curve on the right where F is increasing with ω is unstable in the sense that a slight increase in ω would perturb the front to a condition in which the left hand side of (20) would exceed σ_c^2. One notes immediately that there exists no solution when $\lambda = 1$ since $F \geqslant 0$. In other words, an attached boundary emerging from the end of the cut at some angle is not possible for an ideally brittle interface. By contrast, when $\lambda = 0$

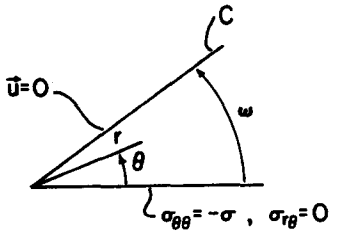

Fig. 6. Geometry at end of cut for local analysis of attached boundary.

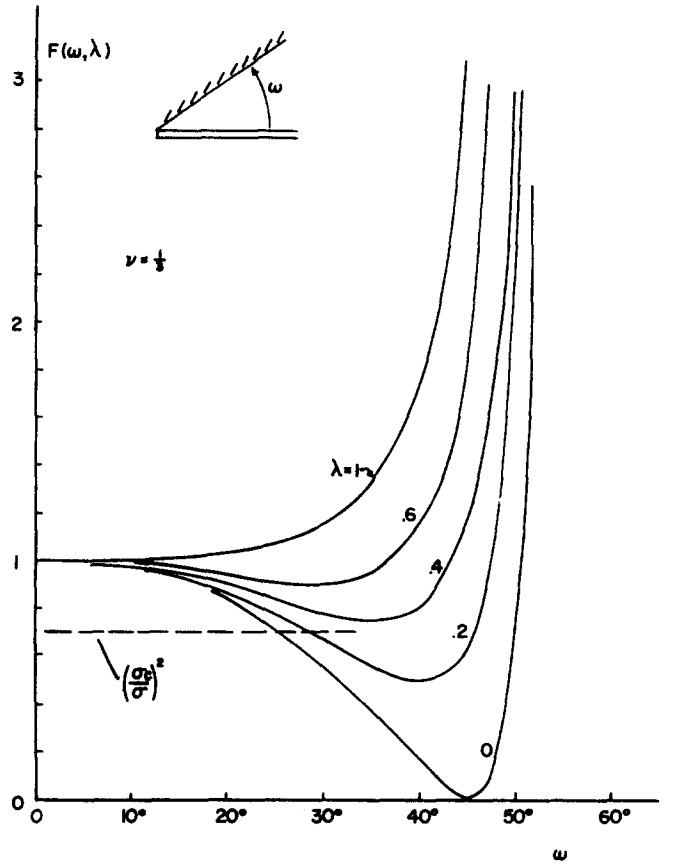

Fig. 7. Function $F(\omega, \lambda)$ associated with local analysis of boundary attached to end of cut. Condition for determining ω is $F = (\sigma_c/\sigma)^2$.

there exists a solution for ω for all $\sigma > \sigma_c$. For $0 < \lambda < 1$, there exists an attached local solution for a range of σ/σ_c, but for σ/σ_c sufficiently large no such solution exists. The numerical results presented in the next section are completely consistent with the conclusions drawn from the local analysis. In fact, it wasn't until this local analysis was conducted that the numerical analysis could be formulated properly.

4. NUMERICAL RESULTS AND COMPARISON WITH SOME OBSERVATIONS

The numerical method used to solve for C made use of a sequence of interations wherein C was adjusted in a systematic manner until (20) was satisfied. In a given iteration with a given C, the plane stress boundary value problem (ii) of Fig. 4 was solved using a finite element procedure which subdivided the region within C into a grid of elements with due attention to achieving resolution near the ends of the cut. The normal and tangential tractions, σ_{nn} and σ_{nt}, on C were determined, the error in (20) was computed, and an adjustment to C for the next iteration was established. Details of this procedure are spelled out in Appendix B. Insight from the local analysis of the previous section was essential in knowing how to deal with the issue of whether C attaches or stands off the end of the cut. Under conditions where C is attached, the numerical prediction for the wedge angle ω was in excellent agreement with the prediction from the local analysis.

One-quarter sections of the computed decohered regions are shown in Fig. 8 for $\lambda = 0$, 1/2 and 1, in each case for $\nu = 1/3$. When mode 3 has no influence on decohesion ($\lambda = 0$), the boundary of the decohered region always remains attached to the ends of the cut. When $\lambda = 1$, the boundary always stands off the end of the cut. Moreover, for a given value of σ/σ_c, the extent of the decohesion is more extensive when $\lambda = 1$ than when $\lambda = 0$. When

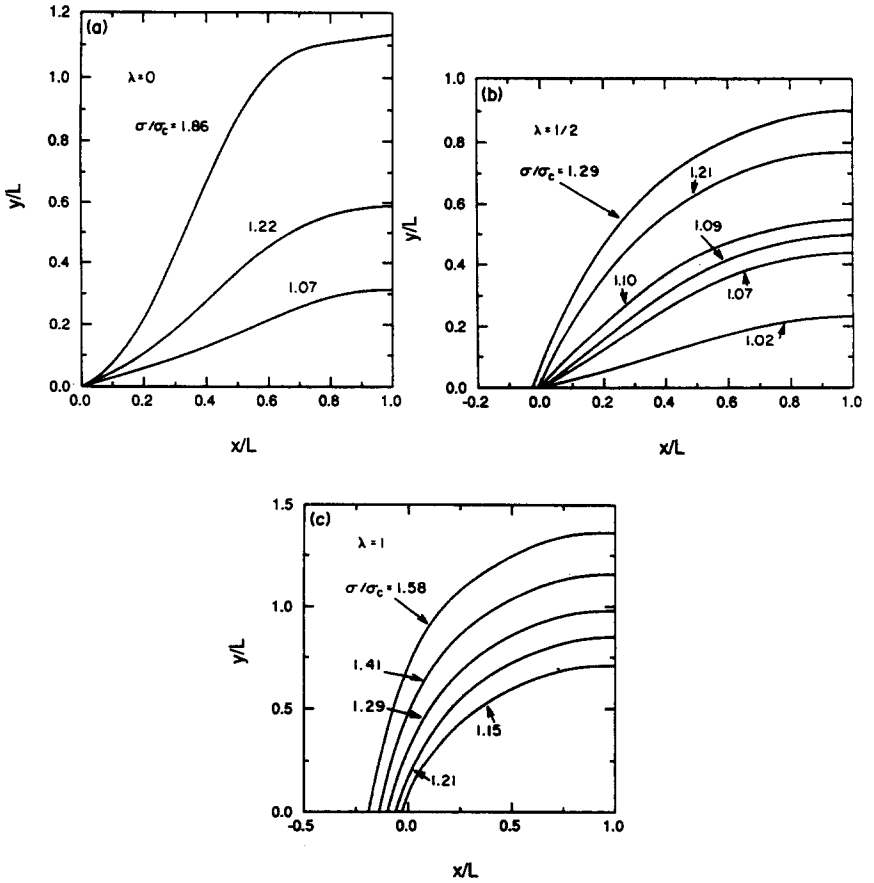

Fig. 8. Computed boundaries of decohered region for various values of σ/σ_c for $\lambda = 0$, 1/2 and 1 with $\nu = 1/3$. The case $\lambda = 0$ applies to a criterion based on $K_1 = K_1^c$ along the boundary independent of K_2 and K_3, while the case $\lambda = 1$ applies to an ideally brittle interface where $\mathcal{G} = \mathcal{G}_c^0$ along the boundary.

$\lambda = 1/2$, the local analysis predicts that the boundary is attached to the ends of the cut for $\sigma/\sigma_c < 1.1$ and stands off for $\sigma/\sigma_c > 1.1$, consistent with the boundaries shown in Fig. 8.

Decohered regions for a thin film of polyimide approximately 35 μm thick and bonded to a glass plate approximately 2 mm thick are shown in Figs 9 and 10. Figure 9 shows decohesion spreading outside a circular cut of about 0.75 cm in radius. (The thin film inside the cut has completely detached.) Figure 10 shows decohesion from a straight cut of approximately 1 cm in length made on the same plate. Each of the two smaller decohered regions below the cut appear to be pinned at a point along the cut, probably because the cut was not as sharp as it should have been on that side. Note, however, that the three shapes are similar.

Information from the extent of the decohered region from the circular cut together with the observed shape of the decohered region in the straight cut test can be used to good advantage to draw conclusions about the nature of the decohesion criterion. For the axisymmetric decohesion boundary induced by the circular cut, $\sigma_{nt} = 0$, by symmetry, so that mode 3 plays no role. The plane stress problem for the circular cut is readily solved (Farris and Bauer, 1988)†. Imposition of the criterion (20) then gives the extent of the decohesion. The ratio, R_0/R_i, of the radius of the decohered region to the radius of the circular cut is found to satisfy

$$\sigma/\sigma_c = \tfrac{1}{2}[(1-\nu)(R_0/R_i)^2 + 1 + \nu]. \tag{26}$$

By measuring the ratio R_0/R_i in Fig. 9 and using $\nu = 1/3$, we determined $\sigma/\sigma_c \cong 1.21$

†We are indebted to Professor R. J. Farris of the University of Massachusetts for supplying us with the polyimide coated glass plate.

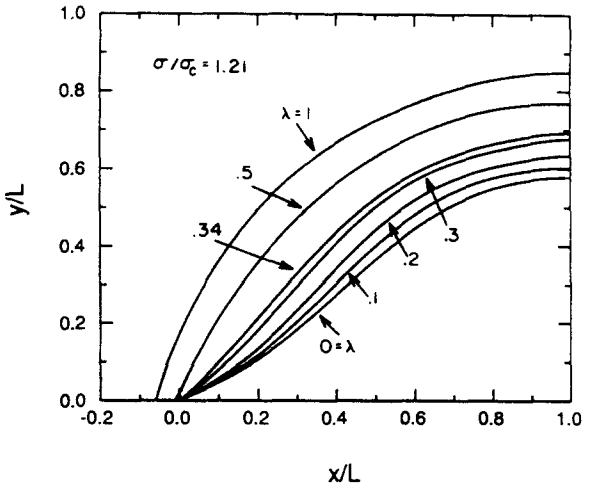

Fig. 11. Computed boundaries of decohered boundaries for $\sigma/\sigma_c = 1.21$ and $\nu = 1/3$ for various values of λ. The value $\sigma/\sigma_c = 1.21$ corresponds to the value of the parameters for the polyimide film/glass plate system in Figs 9 and 10.

from (26). (Note that this procedure enabled us to avoid direct measurement of individual quantities such as E, t, $\mathcal{G}_c^*$, σ, etc.) Next, assuming $\sigma/\sigma_c = 1.21$ and $\nu = 1/3$, we computed the shapes of the decohered region for the straight cut as they depend on λ. These computed shapes are shown in Fig. 11. For $\sigma/\sigma_c = 1.21$ with $\nu = 1/3$, the transition from an attached boundary to one which stands off the ends of the cut occurs at $\lambda = 0.34$. The shape which best approximates the observed shape in Fig. 10 corresponds to $\lambda \cong 0.3$, nearly at the transition to stand-off. With reference to the criterion (20), the value $\lambda \cong 0.3$ for the polyimide/glass interface suggests that mode 3 has a relatively small influence on the interface fracture process. Evidently the tip of the interface crack is heavily shielded from the full effect of mode 3. This finding is consistent with the analogous observations for an epoxy/glass interface under combined modes 1 and 2 (Cao and Evans, 1989). For that system, the tip of the plane strain interface crack was shielded from the effect of mode 2 by a comparable amount.

5. CONCLUDING REMARKS

The residual stress state assumed throughout this paper was equal biaxial tension σ. One can readily verify that the shapes predicted for the equal biaxial residual stress state ($\sigma_{11} = \sigma$, $\sigma_{22} = \sigma$) are unchanged according to the model if the residual stress component parallel to the cut σ_{11} is different from σ, i.e. for ($\sigma_{11} = \sigma_0$, $\sigma_{22} = \sigma$). Observations of decohesion under uniaxial stressing perpendicular to the cut were recently made on a model system where a thin layer of transparent rubber adheres by van-der-Waals forces to a silicone rubber substrate (Ashby and Burwell, 1988).

The shape of the decohered region in the straight cut test is quite sensitive to the extent to which mode 3 enters the decohesion criterion. For a polyimide/glass combination the observed shapes suggest that the interface is far from being "ideally brittle", with significant shielding of the crack tip from the influence of mode 3. This study emphasizes the importance of mode-dependence in interface fracture. A family of decohesion criteria is proposed in Appendix A which is applicable to arbitrary combinations of modes 1, 2 and 3 and which can model the full range of behavior from ideally brittle to fracture controlled by K_1, as long as $K_1 > 0$. We suspect that the least certain aspect of the present model is the use of the criterion (17) when $\Delta\sigma_{nn} > 0$, as it is just opposite the ends of the cut when the decohesion boundary stands off the ends. As discussed in Section 2, the crack front will be closed when $\Delta\sigma_{nn} > 0$ with $K_1 = 0$ and it seems unlikely that (17) should continue to apply, at least not with the same values of λ and $\mathcal{G}_c^*$ as in the range when $\Delta\sigma_{nn} < 0$.

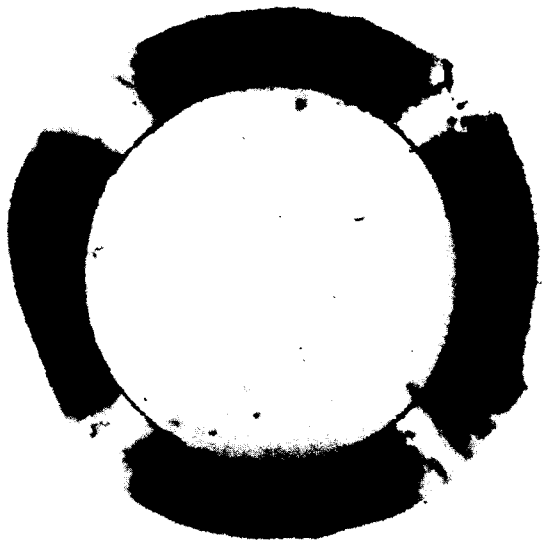

9

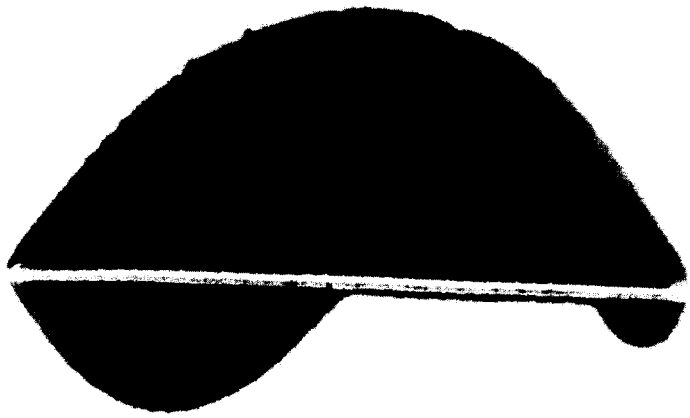

10

Fig. 9. Decohered region exterior to a circular cut on a glass plate with a film of polyimide.

Fig. 10. Decohered regions from a straight cut on a glass plate with a film of polyimide. The plate is the same as that for the circular cut in Fig. 9.

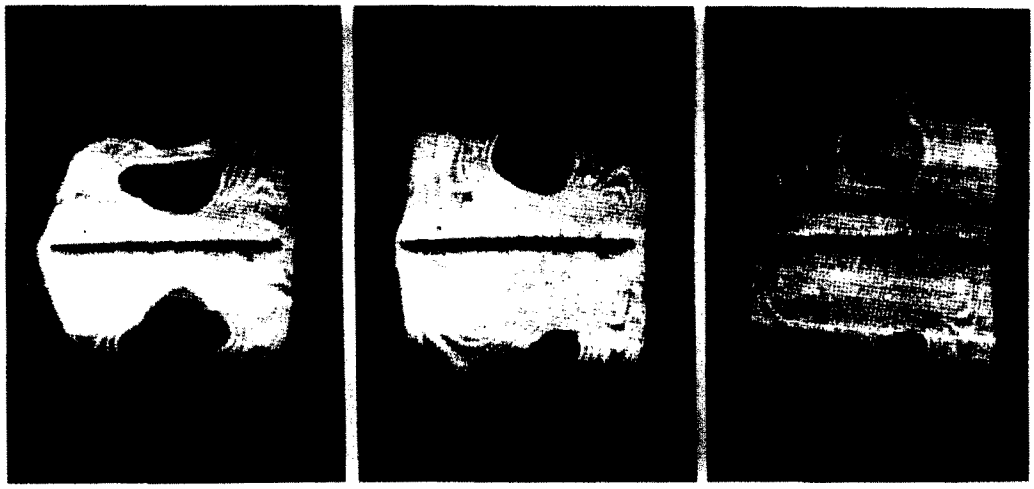

Fig. 13. Decohered regions from cut for a relatively thick polyimide film on glass at three temperatures: $T = 120$ C, 80 C and 40 C. Regions where the film has rebonded to the substrate are evident.

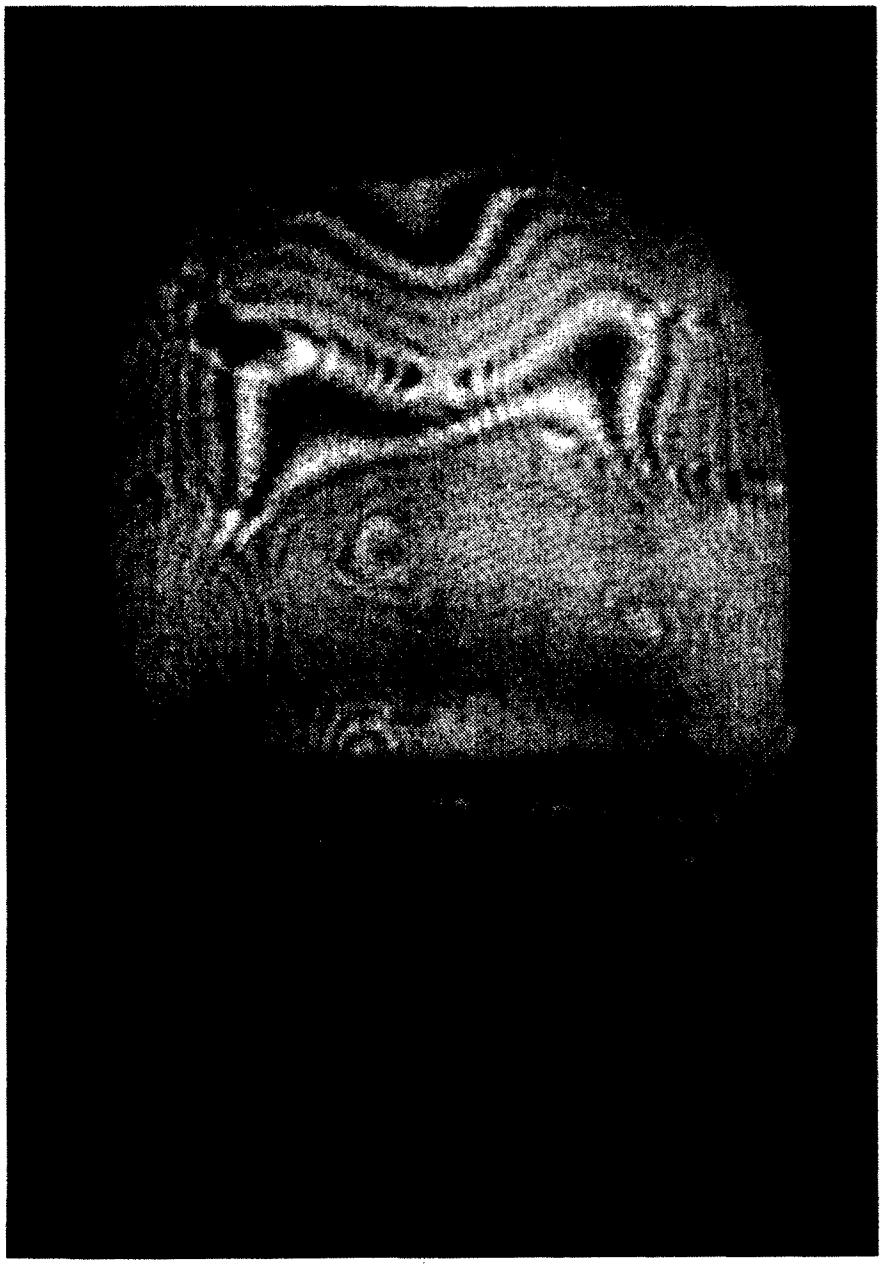

Fig. 14. Decohered region for the relatively thick polyimide film on glass at room temperature.

Further evidence of the complication which occurs when the film comes into contact with the substrate is seen in Figs 13 and 14. The system in these two figures is also a polyimide film on a glass substrate but here the film is almost five times thicker ($t = 150\,\mu m$) than in the system discussed in the previous section. The cut length is approximately 6 mm. In these examples the film was cut at a temperature ($T = 180°C$) at which the residual stress initiates limited decohesion. The specimens are then cooled down. The thermal expansion mismatch between the film and the substrate increases the residual tension in the film as the temperature drops and decohesion spreads. The three decohesion regions shown in Fig. 13 are associated with the three approximate temperatures, $T = 120°C$, 80°C and 40°C, respectively. The decohesion boundary does stand off the ends of the cut by a small amount and, moreover, the crack front is open ($K_1 > 0$) just opposite the cut ends. A second highly noticeable feature in Fig. 13 is the region of contact between the film and the substrate, as indicated by the dark spots more or less in the center of each of the decohered zones. These spots of contact appear to have had a significant influence on the shape of the decohered region, retarding its growth transverse to the cut. Note that the location and size of the contact spots change as the temperature is lowered. On the upper side of the cut one can see the interaction and subsequent merging of the boundary of the decohered region with a small circular decohered region pre-existing prior to the cut having been made.

There is evidence that a fairly substantial residual stress gradient exists in the film in this system with larger tensile stress at the interface than at the surface. A piece of fully decohered film curls consistent with the above observation. This residual stress gradient could account for the crack front remaining open at the ends of the cut and it might have some influence on the tendency of the film to contact the substrate.

Figure 14 shows another example for the same system cooled down to room temperature. The decohered region on one side of the cut is fully developed with no interior contact spots while that on the other side has been retarded by a substantial contact region. If contact occurs in the early stage of the process it seems to persist. Conversely, a decohering region free of interior contact zones tends to avoid contact as it spreads. It is almost as if contact enters the process as an initial condition.

Acknowledgements—This work was supported in part by DARPA University Research Initiative (Subagreement P.O. #VB38639-0 with the University of California, Santa Barbara, ONR Prime Contract N00014-86-K-0753), the Office of Naval Research (Contract N00014-87-K-0493), the National Science Foundation under Grant MSM-88-12779, and the Division of Applied Sciences, Harvard University.

REFERENCES

Ashby, M. F. and Burwell, J. R. (1988). Preliminary results of delamination experiments (private communication).

Cao, H. C. and Evans, A. G. (1989). An experimental study of the fracture resistance of bimaterial interfaces. *Mechanics of Materials* **7**, 295–304.

Evans, A. G., Drory, M. D. and Hu, M. S. (1988) The cracking and decohesion of thin films. *J. Mater. Res.* **3**, 1043–1049.

Evans, A. G. and Hutchinson, J. W. (1989). Effects of non-planarity on the mixed mode fracture resistance of bimaterial interfaces. *Acta Metall.* **37**(3), 909–916.

Farris, R. J. and Bauer, C. L. (1988). A self-delamination method of measuring the surface energy of adhesion of coatings. *J. Adhesion* **26**, 293–300.

Hutchinson, J. W. (1989). Mixed mode fracture mechanics of interfaces. To be published in *Acta Met./Scripta Met. Proceedings of Conference on Metal/Ceramic Interfaces* (Edited by M. Rühle and A. G. Evans). Pergamon, Oxford.

Kinloch, A. J. (1987). *Adhesion and Adhesives*, Chapman and Hall, London, p. 313.

Suo, Z. and Hutchinson, J. W. (1989a). Interface crack between two elastic layers. To be published in *Int. J. Fracture*.

Suo, Z. and Hutchinson, J. W. (1989b). Steady-state cracking in brittle substrates beneath adherent films. *Int. J. Solids and Structures* **25**, 1337–1353.

Thouless, M. D., Cao, H. C. and Mataga, P. A. (1989). Delamination from surface cracks in composite materials. *J. Materials Science* **24**, 1406–1412.

APPENDIX A: A FAMILY OF CRITERIA FOR INTERFACIAL FRACTURE UNDER MIXED MODE

Noting the expression (14) for the energy release rate of the interface crack under all three modes of loading (with $\beta = 0$), consider the family of interface toughness criteria specified by

$$\frac{1}{2}\left(\frac{1-\nu^2}{E}+\frac{1-\nu_s^2}{E_s}\right)(K_1^2+\lambda_2 K_2^2)+\frac{\lambda_3}{4}\left(\frac{1}{\mu}+\frac{1}{\mu_s}\right)K_3^2=\mathcal{G}_c^0 \tag{A1}$$

where $\mathcal{G}_c^0$ can be regarded as the pure mode 1 toughness. The parameters λ_2 and λ_3 adjust the extent to which the shearing modes, K_2 and K_3, affect decohesion; they are limited to a range between 0 and 1. It is assumed that $K_1 > 0$. For given values of λ_2 and λ_3, this criterion can be rewritten as

$$\mathcal{G}=\mathcal{G}_c(\psi,\phi) \tag{A2}$$

where ψ and ϕ are Euler angles in the space (K_1, K_2, kK_3), as shown in Fig. 12, and where

$$\mathcal{G}_c(\psi,\phi)=\mathcal{G}_c^0[1+(\lambda_2-1)\sin^2\psi\sin^2\phi+(\lambda_3-1)\cos^2\phi]^{-1}. \tag{A3}$$

In casting the criterion in the form (A2), it has been mathematically convenient to scale the K_3-axis by k where

$$k^2=\frac{1}{2}\left(\frac{1}{\mu}+\frac{1}{\mu_s}\right)\left[\frac{1-\nu^2}{E}+\frac{1-\nu_s^2}{E_s}\right]^{-1}. \tag{A4}$$

This family of criteria includes the following special cases.

(i) "Ideally brittle" decohesion:

$$\lambda_1=\lambda_2=1, \quad \mathcal{G}_c=\mathcal{G}_c^0. \tag{A5}$$

(ii) Decohesion independent of the shearing modes (i.e. $K_1=K_1^c$):

$$\lambda_1=\lambda_2=0, \quad \mathcal{G}_c=\mathcal{G}_c^0[1-\sin^2\psi\sin^2\phi-\cos^2\phi]^{-1} \tag{A6}$$

where $\mathcal{G}_c^0$ is the pure mode 1 toughness related to K_1^c by (A1) with $K_2=K_3=0$.

(iii) The decohesion criterion (17) used in the body of the present paper is included in (A2) if one makes the identification

$$\lambda=\lambda_3[1+(\lambda_2-1)\sin^2\psi]^{-1}, \quad \mathcal{G}_c^*=\mathcal{G}_c^0[1+(\lambda_2-1)\sin^2\psi]^{-1}. \tag{A7}$$

Thus, a solution in the body of the paper for a given pair $(\lambda, \mathcal{G}_c^*)$ corresponds to a solution for any combination of $(\lambda_2, \lambda_3$ and $\mathcal{G}_c^0)$ satisfying (A7). For example, the solution for $\lambda=0$ applies to an interface with $\lambda_2=\lambda_3=0$ and $\mathcal{G}_c^*=\mathcal{G}_c^0$, but it also applies to any interface with $\lambda_3=0$ and $\lambda_2\neq 0$ if $\mathcal{G}_c^*=\mathcal{G}_c^0[1+(\lambda_2-1)\sin^2\psi]^{-1}$.

A comparison of (A1) with the Cao–Evans (1989) mode 1/mode 2 data for epoxy on glass is shown in Fig. 15. The choice $\lambda_2=0.15$ gives a reasonable fit to this data. Now suppose that the value $\lambda_2=0.15$ applies as well

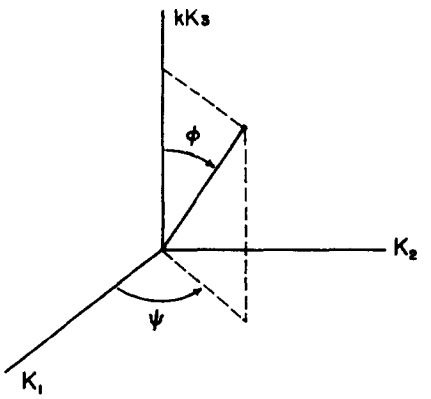

Fig. 12. Definition of Euler angles in (K_1, K_2, kK_3)-space.

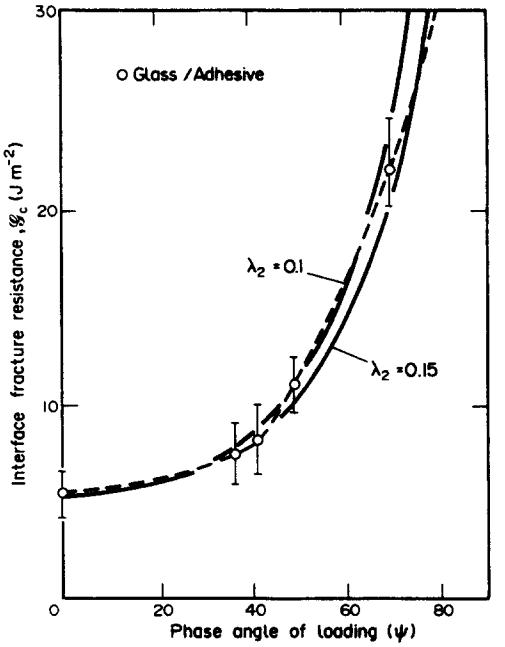

Fig. 15. Comparison of the Cao–Evans (1989) data for an epoxy/glass interface with the phenomenological criterion (A1) for two values of λ_2.

to the polyimide/glass system used in the present study. With $\lambda = 0.3$ inferred from the shape of the decohesion in the cut test and with $\psi = 50°$, Eqn (A7) gives $\lambda_3 = 0.15$. Thus it would appear that the polyimide/glass interface crack is heavily shielded from both mode 2 and mode 3 by comparable amounts.

The criterion (A1) can be expressed in a form which has been considered in the adhesives literature (Kinloch, 1987). When $\beta = 0$, separate "components" of the energy release rate can be meaningfully defined as

$$(\mathcal{G}_1, \mathcal{G}_2) = \frac{1}{2}\left(\frac{1-\nu^2}{E} + \frac{1-\nu_s^2}{E_s}\right)(K_1^2, K_2^2)$$

$$\mathcal{G}_3 = \frac{1}{4}\left(\frac{1}{\mu} + \frac{1}{\mu_s}\right)K_3^2. \tag{A8}$$

Then it is immediately noted that (A1) can be rewritten as

$$\frac{\mathcal{G}_1}{\mathcal{G}_1^c} + \frac{\mathcal{G}_2}{\mathcal{G}_2^c} + \frac{\mathcal{G}_3}{\mathcal{G}_3^c} = 1 \tag{A9}$$

where $\mathcal{G}_1^c \equiv \mathcal{G}_c^0, \mathcal{G}_2^c = \mathcal{G}_c^0/\lambda_2$ and $\mathcal{G}_3^c = \mathcal{G}_c^0/\lambda_3$. In this form, $\mathcal{G}_2^c$ and $\mathcal{G}_3^c$ are regarded as the pure mode toughnesses. The intention behind (A1) is that mode 2 and mode 3 act together with mode 1. It is not necessarily expected that (A1) should accurately span the whole range of behavior to include pure mode 2 or mode 3.

APPENDIX B: NUMERICAL METHOD

The plane stress problem is Problem (ii) of Fig. 4, with boundary conditions (12). The boundary C of the decohered region must be found such that (20) holds along C where σ_{nn} and σ_{nt} are the normal and tangential stresses to C from Problem (ii).

For a given shape, the stresses are determined using the finite element method. A coarse mesh (4×3) is shown in Fig. 16a. Typically, a (30×30) mesh gave results of sufficiently high accuracy. Each quadrilateral consists of two linear displacement elements with straight edges.

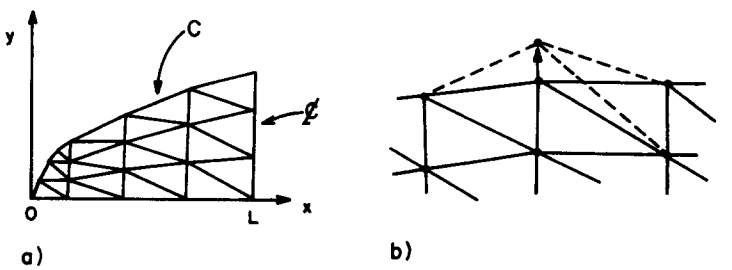

Fig. 16. (a) Finite element grid. (b) Movement of boundary node.

Two methods for representing a boundary shape that locally satisfies the decohesion criterion have been compared. Both methods lead to an iterative procedure.

In the first method, the boundary curve C is represented by a set of functions according to

$$y(x) = a_0 + a_1 f_1(x) + a_2 f_2(x) + \cdots + a_N f_N(x). \tag{B1}$$

Let $x = 0$ be at the end of the cut and $x = L$ at the symmetry line at the center of the cut as indicated in Fig. 16a. The following polynomial expansion is used

$$\begin{aligned} f_1(t) &= t(2-t), \quad f_2(t) = t^2(3-2t), \\ f_n(t) &= t^2(t-1)^2 T_{n-3}(2t-1) \quad 3 \leqslant n \leqslant N \end{aligned} \tag{B2}$$

where $t = x/L$ and T_n are Chebyshev polynomials of order n.

For the case where the decohesion zone stays attached, $a_0 = 0$ in (B1) and the results of the FEM analysis and the local analysis of Section 3 can be compared. The angle between the cut and the decohesion zone as given by the two methods is usually within 0.5%.

In the second method, the boundary curve is represented by a piecewise linear curve as in the FEM approximation in Fig. 16a. The boundary is in this way described by a set of coordinates (x_p, y_p), $p = 1, 2, \ldots, P$, with a linear variation between these points.

Let the initial boundary curve be represented by polynomials as in the first method above. The criterion (20) is approximately satisfied along C by choosing the coefficients a_i to minimize

$$E_{rr} = \int_C \left[\sigma_c^2 - \left\{ \sigma_{nn}^2 + \frac{2\lambda}{(1-\nu)} \sigma_{nt}^2 \right\} \right]^2 \mathrm{d}s. \tag{B3}$$

The derivatives and curvatures of E_{rr} with respect to each of the a_i are obtained numerically by solving the FEM problem for $a_i + \delta a_i$ and $a_i - \delta a_i$. In an iteration, new values of a_i are found by choosing δa_i to minimize E_{rr} according to the derivatives and curvatures so obtained. In this way, the iteration process usually converges in 5 iterations.

Now let the boundary curve C be represented by the finite element grid as in the second method above. The stress change for a small movement of a nodal point is found for each node on the boundary curve. Use is made of the fact that the FEM grid is unchanged except in three elements, as shown in Fig. 16b, resulting in a nearly unchanged stiffness matrix. The nodes at the boundary are then moved to satisfy the decohesion criterion (20) in each element at the boundary. Since the stress change at C is nonlinear with respect to movements of the nodes of C, the process is iterative. Nodes are moved with x_p kept fixed except when y is small close to the ends of the cut where y_p is kept fixed.

The two methods outlined above result in essentially identical shapes of the decohesion zone. Typically, $N = 4$ in (B1) is sufficient, since results for $N = 6$ usually are indistinguishable. In the cases when the decohesion zone stands off the end of the cut, the set of functions (B2) is used in (B1) for $0 \leqslant x \leqslant L$. For $x < 0$, C is represented by

$$y(x) = c_1 (x - c_2)^{1/2}. \tag{B4}$$

with the c_1 chosen to ensure continuity and smoothness of C at $x = 0$. The symmetry condition at $y = 0$ is then fulfilled. The procedure employed first involved minimizing E_{rr} with respect to the a_i's. Then the nodal points near the end of the cut are adjusted according to the second method in order to lower the error on this part of the curve.

No special treatment of the singular behavior at the ends of the cuts was made, other than focussing the FEM grid towards the end of the cut and comparing results for different levels of discretization.